Gain-of-function mutations in a member of the Src family kinases cause autoinflammatory bone disease in mice and humans

Koichiro Abe[a,1,2], Allison Cox[b,1], Nobuhiko Takamatsu[c], Gabriel Velez[d,e], Ronald M. Laxer[f], Shirley M. L. Tse[f], Vinit B. Mahajan[d], Alexander G. Bassuk[b], Helmut Fuchs[g], Polly J. Ferguson[b,3], and Martin Hrabe de Angelis[g,h,i,3]

[a]Department of Molecular Life Science, Tokai University School of Medicine, Isehara 259-1193, Kanagawa, Japan; [b]Department of Pediatrics, University of Iowa Carver College of Medicine, Iowa City, Iowa, IA 52242; [c]School of Science, Kitasato University, Sagamihara 252-0373, Kanagawa, Japan; [d]Omics Laboratory, Byers Eye Institute, Stanford University, Palo Alto, CA 94304; [e]Medical Scientist Training Program, University of Iowa Carver College of Medicine, Iowa City, IA 52242; [f]Department of Pediatrics, Hospital for Sick Children, University of Toronto, ON M5G 1X8, Canada; [g]Institute of Experimental Genetics, Helmholtz Zentrum München, 85764 Neuherberg, Germany; [h]Chair of Experimental Genetics, School of Life Science Weihenstephan, Technische Universität München, 85354 Freising, Germany; and [i]German Center for Diabetes Research, 85764 Neuherberg, Germany

Edited by David R. Beier, Seattle Children's Research Institute, Seattle, MA, and accepted by Editorial Board Member Kathryn V. Anderson May 7, 2019 (received for review November 20, 2018)

Autoinflammatory syndromes are characterized by dysregulation of the innate immune response with subsequent episodes of acute spontaneous inflammation. Chronic recurrent multifocal osteomyelitis (CRMO) is an autoinflammatory bone disorder that presents with bone pain and localized swelling. *Ali18* mice, isolated from a mutagenesis screen, exhibit a spontaneous inflammatory paw phenotype that includes sterile osteomyelitis and systemic reduced bone mineral density. To elucidate the molecular basis of the disease, positional cloning of the causative gene for *Ali18* was attempted. Using a candidate gene approach, a missense mutation in the C-terminal region of *Fgr*, a member of Src family tyrosine kinases (SFKs), was identified. For functional confirmation, additional mutations at the N terminus of *Fgr* were introduced in *Ali18* mice by CRISPR/Cas9-mediated genome editing. N-terminal deleterious mutations of *Fgr* abolished the inflammatory phenotype in *Ali18* mice, but in-frame and missense mutations in the same region continue to exhibit the phenotype. The fact that *Fgr* null mutant mice are morphologically normal suggests that the inflammation in this model depends on Fgr products. Furthermore, the levels of C-terminal negative regulatory phosphorylation of Fgr^{Ali18} are distinctly reduced compared with that of wild-type Fgr. In addition, whole-exome sequencing of 99 CRMO patients including 88 trios (proband and parents) identified 13 patients with heterozygous coding sequence variants in *FGR*, including two missense mutant proteins that affect kinase activity. Our results strongly indicate that gain-of-function mutations in *Fgr* are involved in sterile osteomyelitis, and thus targeting SFKs using specific inhibitors may allow for efficient treatment of the disease.

chronic recurrent multifocal osteomyelitis | autoinflammation | mouse model | tyrosine kinase | bone destruction

Autoinflammatory syndromes are disorders of innate immunity characterized by episodes of seemingly unprovoked sterile inflammation without increased autoantibodies or involvement of self-reactive lymphocytes (1). Many autoinflammatory disorders have a monogenic basis, but for most, a combination of genetic and environmental factors contributes to disease susceptibility. Chronic recurrent multifocal osteomyelitis (CRMO), also known as chronic nonbacterial osteomyelitis (CNO), is an autoinflammatory bone disease which presents with bone pain and local swelling due to unifocal, or more often multifocal sites of sterile osteomyelitis (2–5). While the genes for two syndromic forms of CRMO (*LPIN2* and *IL1RN*) are known (6, 7), the genetic etiology for nonsyndromic CNO/CRMO is poorly understood.

A forward genetics approach using animal models is a powerful tool for the molecular dissection of pathogenesis in inflammatory bone diseases (8). Examples include *Pstpip2* (*lupo* and *cmo* mice) (9–11) and *Zap70* (*skg* mice) (12), which were identified and well characterized without human disease data. Further, similar autoinflammatory phenotypes of *Ali5* (13) and *Ali14* (14) mice caused by missense mutations in *phospholipase C gamma* (*Plcg2*) are related to the novel human hereditary disease PLAID (PLCG2-associated antibody deficiency and immune dysregulation) (15, 16). However, most of the intracellular cascades which lead to autoinflammatory diseases are not well known.

The *Ali18* mutant mouse strain was isolated in the Munich ENU mutagenesis project because of paw inflammation (Fig. 1*A*) (17). *Ali18* mice show synovitis, sterile osteomyelitis, and systemic reduced bone mineral density, particularly in trabecular areas of long bones (17). Because these phenotypes are reconstituted by bone marrow transfer and are independent of mature lymphocytes (18), *Ali18* mice are considered a mouse model of autoinflammatory bone disease. Although the *Ali18* locus was mapped to mouse chromosome 4 by standard genetic mapping, complex modifier effects hinder its precise determination (19). In this study, positional candidate cloning identified *Fgr*, a member of Src family kinases, as the causative gene

Significance

Chronic recurrent multifocal osteomyelitis (CRMO) is an autoinflammatory bone disease that presents with bone destruction occurring primarily in children. In a mouse ENU mutagenesis screen, the *Ali18* strain was isolated because of spontaneous inflammation in the joints and bones. Sequencing candidate genes in the *Ali18* critical region identified a missense mutation in the C-terminal regulatory region of the Src family kinase (SFK) member, *Fgr*. Genome editing revealed *Fgr* dependency of the inflammatory phenotype in *Ali18* mice. Further, whole exome sequencing in our CRMO cohort identified two patients with missense mutations in *FGR*. In vitro functional assays confirm altered protein function. This work identifies *FGR* as a CRMO susceptibility gene and suggests that targeting SFKs may be useful in its treatment.

Author contributions: K.A., P.J.F., and M.H.d.A. designed research; K.A., A.C., N.T., G.V., R.M.L., S.M.L.T., H.F., P.J.F., and M.H.d.A. performed research; K.A., A.C., N.T., G.V., R.M.L., S.M.L.T., V.B.M., A.G.B., H.F., and P.J.F. analyzed data; and K.A., A.C., N.T., A.G.B., P.J.F., and M.H.d.A. wrote the paper.

The authors declare no conflict of interest.

This article is a PNAS Direct Submission. D.R.B. is a guest editor invited by the Editorial Board.

[1]K.A. and A.C. contributed equally to this work.

[2]To whom correspondence may be addressed. Email: abeko@is.icc.u-tokai.ac.jp.

[3]P.J.F. and M.H.d.A. contributed equally to this work.

This article contains supporting information online at www.pnas.org/lookup/suppl/doi:10.1073/pnas.1819825116/-/DCSupplemental.

Published online May 28, 2019.

for *Ali18*. Further, two other missense mutations in *FGR* were found in our cohort of patients with CRMO.

Results

***Ali18* Mice, Fine Mapping, and Candidate Resequencing.** By standard genetic mapping, we narrowed down the critical region to ∼3 Mb utilizing recombination between wild-type and heterozygous/homozygous genotypes (Fig. 1*B* and *SI Appendix*, Table S1). In the identified region, we focused on 16 candidate genes using a literature-based search engine, PosMed (20). By sequencing the exonic region of these genes by the Sanger method, we found a mutation, c.1506A > G, in the protein coding region of the Gardner-Rasheed feline sarcoma viral (v-Fgr) oncogene homolog (*Fgr*) gene (21) (Fig. 1*C*). Digestion of PCR products encompassing exon 13 of *Fgr* by Mbo II restriction enzyme, which recognizes the wild-type allele (5′-GAAGA-3′) but not c.1506A > G (5′-GAAGG-3′), produces longer DNA fragments in *Ali18* mice (Fig. 1*D*). Genotype–phenotype correlations revealed that the mutation was not present in unaffected littermates or wild-type controls.

A Member of SFK as the Top Candidate for the Causative Gene. Fgr is a member of the Src family kinases (SFKs), which share the SH2, SH3, and catalytic domains with high homology to other family members (22), and the c.1506A > G mutation causes an amino acid change (p.Asp502Gly) in the terminal end of the catalytic domain (Fig. 1*E*). Alignment of the amino acid sequences of Fgr with those of other SFKs indicates that the 502 aspartic acid is conserved among Src, Fyn, Yes, Lyn, and Lck (Fig. 1*F*). The corresponding amino acid in Hck and Blk is glutamic acid and has a negatively charged side chain as does aspartic acid. The aspartic acid of Fgr is also conserved in humans (Fig. 1*F*, FGR). We searched sequence variants among 36 mouse inbred strains in the "mousepost.be" database (23) and no variants were detected in the *Fgr* locus. The PROVEAN (Protein Variation Effect Analyzer) software (24) predicts that the amino acid substitution is deleterious (score = −6.440; cutoff = −2.5). In addition, we performed whole-genome sequencing by next generation sequencer (NGS) using genomic DNA from *Ali18*/+ and wild-type mice on the same genetic background, and *Fgr* c.1506A > G (IGV_2.3.94, mouse mm10, chr4: 133,000,294, *SI Appendix*, Fig. S1*A*) mutations were found in only *Ali18*/+ DNA as a heterozygous change (NGS reads, A:20 and G:24). Within the *Ali18* critical region, we found three other candidate mutations (IGV_2.3.94, mouse mm10, chr4: 133,543,428; chr4: 133,705,306; chr4: 133,919,389, *SI Appendix*, Fig. S1 *B*–*D*) besides the *Fgr* coding mutation. However, all three mutations are located in noncoding regions.

Deficiency of Fgr Abolishes the Autoinflammatory Phenotype of *Ali18* Mice. To confirm whether the inflammatory phenotype of *Ali18* mice is caused by the *Fgr* coding mutation, we used the prokaryotic antiviral system, CRISPR/Cas9, to induce additional loss-of-function mutations in the N-terminal region of Fgr besides p.Asp502Gly. Because *Fgr* knockout mice show no overt phenotype (25, 26), it is predicted that loss-of-function mutations in *Fgr* do not support the osteomyelitis phenotype in *Ali18* mice. As shown in Fig. 2 *A* and *B*, two pX330 related constructs containing guide RNA around exon 3 of the *Fgr* gene (fgRNA1 and -2) were microinjected into *Ali18*/*Ali18* fertilized eggs. Therefore, all of the *Cas9*-induced mutations are in the *Ali18* haplotype containing the *Fgr* c.1506A > G/p.Asp502Gly mutation (Fig. 2*A*). In the founder (F0) generation, we sequenced the region flanking and including exon 3 which contains the transcriptional initiation site of *Fgr*. All F0 mice (nos. 405, 406, 407, 409, 410, and 411) without mutation around the *Cas9*-targeted PAM sites exhibit the arthritic phenotype (6/6). In contrast, half of the F0 mice harboring mutations around the PAM sites did not show the inflammatory paw phenotype (5/10).

As it is expected that somatic and germ cells of the F0 mice are chimeric with various indel mutations around the PAM, we crossed F0 mice with wild-type C3HeB/FeJ mice to obtain F1 mice without chimerism (Fig. 2*B*). Twelve germline-transmitted lines were established from seven F0 mice with a mutation around PAM (*SI Appendix*, Table S2). Among all 12 lines established, 8 lines, which have deleterious mutations in the *Fgr* coding region, such as frameshift (#404a, #404b, #415a, and #416a) and deletion of translational initiation site (#418) and/or splicing acceptor (#417a and #419), abolish the inflamed paw phenotype of *Ali18* mice (Fig. 2 *C* and *D* and *SI Appendix*, Figs. S2 and S3). In contrast, the other four lines with missense (#408 and #416b), in-frame (#415b), and synonymous (#417b) mutations of *Fgr* exhibit the inflammatory paw phenotype (Fig. 2 *C* and *D* and *SI Appendix*, Figs. S2 and S3 and Table S2).

Interestingly, #408a and #417b F1 mice showed different severity of paw swelling compared with original *Ali18* mice. *Ali18*_#408a (p.Ser25Arg;Asp502Gly) (Fig. 2*D* and *SI Appendix*, Fig. S2*C*) mice show more severely inflamed paws, indicating that combination of the amino acid exchanges enhances paw swelling. The #417b (Fig. 2*C*

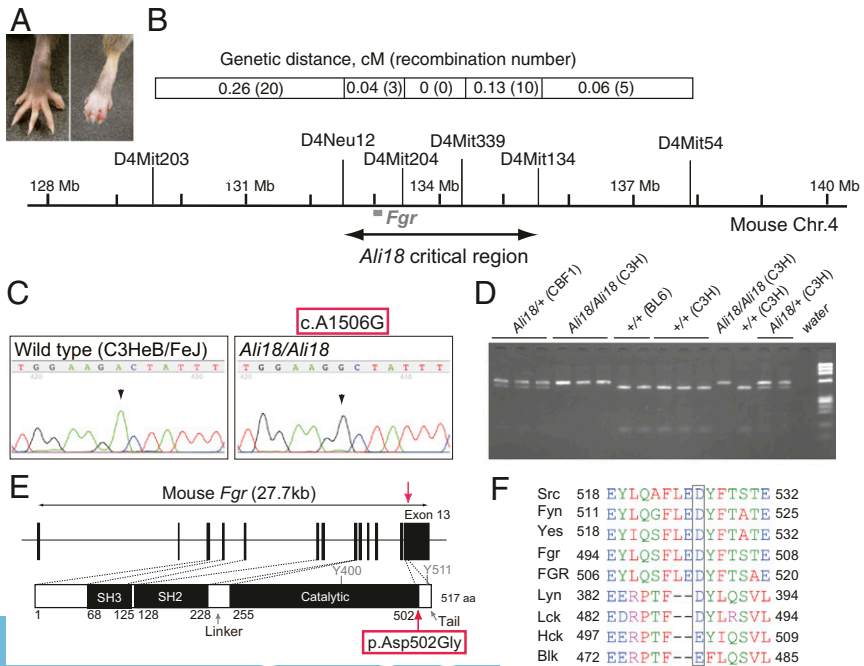

Fig. 1. Positional candidate cloning of the *Ali18* mutation. (*A*) *Ali18*/+ (*Right*) and wild-type C3HeB/FeJ (*Left*) hind paws. *Ali18* mice show reddening and swelling in peripheral paws. (*B*) Genetic map and the critical interval of the *Ali18* locus. The complex modifier effects from the C57BL/6J genetic background prevented further narrowing down of the region. (*C*) By Sanger sequencing of candidate genes in the region, a point mutation (c.1506A > G) in exon 13 of *Fgr*, a member of the SFKs, was detected. (*D*) Mbo II restriction enzyme digestion of PCR products spanning exon 13 correlated to the swollen paw phenotype. Genetic background is described as C3H (C3HeB/FeJ), BL6 (C57BL/6J), and CBF1 (F1 from C3H and BL6 crossing). *Ali18* mice were originally derived from C3H parents. (*E*) Schematic diagram of the p.Asp502Gly (D502G) amino acid change induced by c.1506A > G. Y400 and Y511 indicate the autophosphorylation site and the C-terminal regulatory phosphorylation site, respectively. (*F*) Alignment of Src family tyrosine kinases. Square encompasses the amino acid residues exchanged by the c.1506A > G mutation.

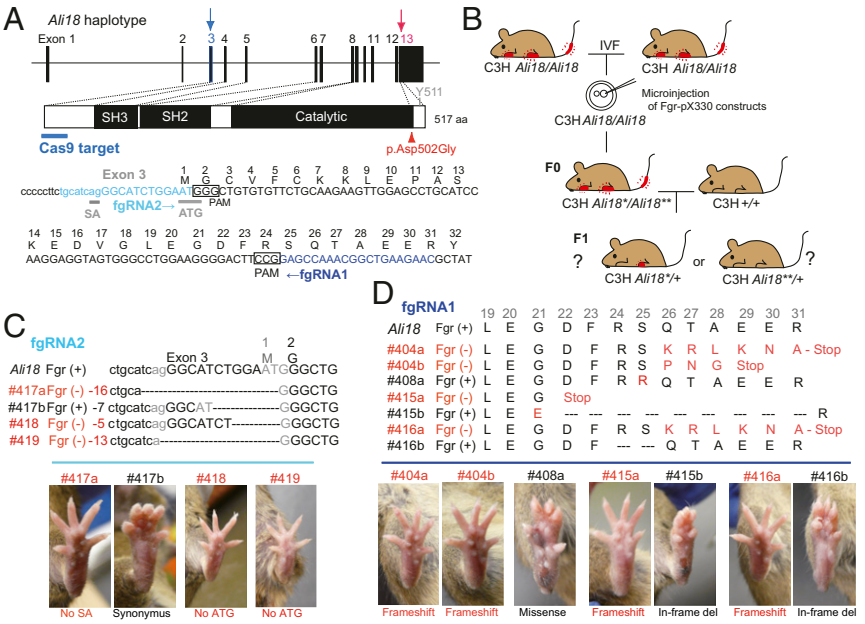

Fig. 2. Disruption of the *Fgr* gene by genome editing alters the autoinflammatory phenotype in *Ali18* mice. (*A*) DNA sequence of guide RNA (fgRNA1 and fgRNA2) and PAM around exon 3 of *Fgr* are indicated. The p.Asp502Gly mutation in exon 13 is also shown. Sanger sequencing of a PCR fragment around exon 3 and genotyping of p.Asp502Gly were done using genomic DNA from F0 and F1 mice. (*B*) Schematic strategy of genome editing in the *Fgr* locus of *Ali18* mice. pX330-based constructs were microinjected into *Ali18/Ali18* oocytes in C3H (C3HeB/FeJ) genetic background from in vitro fertilization. The founder mice (F0) derived from microinjection were bred with wild-type C3H mice to obtain F1 mice. (*C* and *D*) Correlation of *Fgr* genotypes and lower limb morphology of F1 mice. Loss-of-function mutations show no morphological abnormality (red font). In contrast, missense, in-frame deletion, and synonymous mutations exhibit autoinflammatory paws. SA, splice acceptor; ATG, the translational initiation site. See also *SI Appendix*, Table S2 for detail.

and *SI Appendix*, Fig. S2*I*) line, which has an in-frame 5′ UTR deletion with a newly formed ATG codon in *Fgr*, showed swollen paws. However, not all mice of the #417b line showed a swollen paw phenotype (4/9, *SI Appendix*, Table S2 and Fig. S3). It is likely that the newly formed translational initiation site or deletion in the UTR region causes low transcriptional and/or translational efficiency of the Fgr protein. These results strongly support that the *Fgr* p.Asp502Gly mutation is responsible for autoinflammation in *Ali18* mice.

Abnormal C-Terminal Phosphorylation of Fgr^{Ali18} Reveals Gain of Function. To elucidate how the p.Asp502Gly mutation affects Fgr function, we analyzed the tyrosine kinase activities of wild-type and p.Asp502Gly Fgr proteins by standard kinase assay using radioisotope-labeled ATP. Fig. 3*C* shows tyrosine kinase activity of in vitro translated Fgr proteins against affinity purified enolase as a substrate of SFKs. Unlike oncogenic mutations, the kinase activity of p.Asp502Gly Fgr was not dramatically changed. These results were also supported by Western blot analysis using antiphosphotyrosine in *Ali18/Ali18* organs and Fgr p.Asp502Gly expressing cultured cells (Fig. 3 *A* and *B*). We then focused on efficiency of the C-terminal phosphorylation, because p.Asp502Gly is located close to this phosphorylation site. SFKs are normally inactive with the C-terminal phosphorylation by C-terminal Src kinase (Csk, another member of SFKs). To detect the C-terminal phosphorylation, a kinase-ablation mutation (KD, kinase dead) is necessary to avoid autophosphorylation of Src (27). Therefore, we used affinity purified Fgr protein with a p.Lys279Met (K279M) kinase dead mutation ($Fgr_{KD,}$ WT) and Fgr_{KD} with the p.Asp502Gly mutation ($Fgr_{KD}^{Asp502Gly}$, mut) as substrates for kinase assays by Csk. As shown in Fig. 3*D*, specifically phosphorylated products were detected in the samples containing Csk without autophosphorylation. Further, the efficiency of phosphorylation of Fgr_{KD} (WT) by Csk is approximately two times more than that of $Fgr_{KD}^{Asp502Gly}$ (mut) (relative activity ratio: 0.472 ± 0.072). The decrease of C-terminal phosphorylation indicates that $Fgr^{Asp502Gly}$ is more active than wild-type protein. These results strongly suggest that p.Asp502Gly is a gain-of-function mutation of the Fgr tyrosine kinase.

***FGR* Coding Variants Were Detected in Autoinflammatory Bone Disease Patients.** As part of a human CRMO genetic study, whole-exome sequencing by NGS was performed on 99 affected individuals and their family members. The families included 88 family trios (affected and both unaffected parents) and 11 dyads (affected and one unaffected parent). *FGR* variants from affected subjects were queried, and 11 rare exonic variants in total were identified in 13 probands (*SI Appendix*, Table S3). These include two missense variants, p.Arg118Trp and p.Pro525Ser (Fig. 4*H*). For the patient with the p.Arg118Trp mutation, radiographs show osteolytic lesion with sclerosis and periosteal reaction in distal femur (Fig. 4 *A* and *B*) which demonstrated abnormal signal intensity and enhancement on postcontrast MRI compatible with CRMO; an additional MRI shows abnormal inflammation detected in the sacroiliac joint by short-tau inversion recovery (STIR) (Fig. 4*C*).

Genomic DNA from the patient and parents was validated by Sanger sequencing, and the chromatograms indicate a de novo mutation in the child with the p.Arg118Trp *FGR* mutation (Fig. 4*D*). A p.Pro525Ser variation is detected in another child for which DNA from only one parent was available, so it is not known if the variant is inherited or de novo. MRI abnormalities in the fibula of the child are shown in Fig. 4 *E*–*G*. Both variants are rare (*SI Appendix*, Table S3); the p.Arg118Trp (rs774209795) and p.Pro525Ser (rs143850913) variants have minor allele frequencies of 1.2×10^{-5} and 3.5×10^{-4}, respectively, according to gnomAD (28). The PROVEAN software predicts that both amino acid substitutions are deleterious; the score of p.Arg118Trp is −5.015 (cutoff = −2.5); the score of p.Pro525Ser is −2.716 (cutoff = −2.5) and the other predictors including SIFT, Polyphen2, and CADD also predict pathogenicity (*SI Appendix*, Table S5). There were no mutations in the known CRMO susceptibility genes including *FBLIM1*, *IL1RN*, *LIPIN2*, or *PSTPIP2* in these two patients (*SI Appendix*, Table S3). However, the same missense variant in *FBLIM1* was found in two patients with FGR splice or synonymous mutations, and a missense mutation in *LIPIN2* was detected in a patient with an *FGR* 5′ UTR mutation (*SI Appendix*, Tables S3 and S4). All three variants are *in trans* with the coding *FGR* variant based on parental genotypes. The *FBLIM1* variant identified in two probands induces a p.Gly311Arg amino acid change and the *LPIN2* variant induces a p.Cys874Phe change.

To elucidate functional abnormality of the variants found in CRMO patients, kinase assay experiments were performed using affinity purified mutant FGR proteins and enolase (Fig. 4 *I* and *J*). The p.Arg118Trp FGR protein (RW, Fig. 4*H*) show decreased phosphorylation compared with that of wild-type protein (WT) (relative activity ratio: 0.39 ± 0.12, $P < 0.0001$, *t* test, Fig. 4 *I and J*). As shown in *SI Appendix*, Figs. S4 and S5, the structural model of p.Arg118Trp may lead to disruption of SH3-kinase linker interaction which destabilizes the protein functions (see also *SI Appendix*, *Results and Discussion*). In contrast, p.Pro525Ser (PS, Fig. 4*H*) may inhibit the closed-inactive formation of FGR as predicted by the structural model (*SI Appendix*, Fig. S6). Actually, the kinase assay

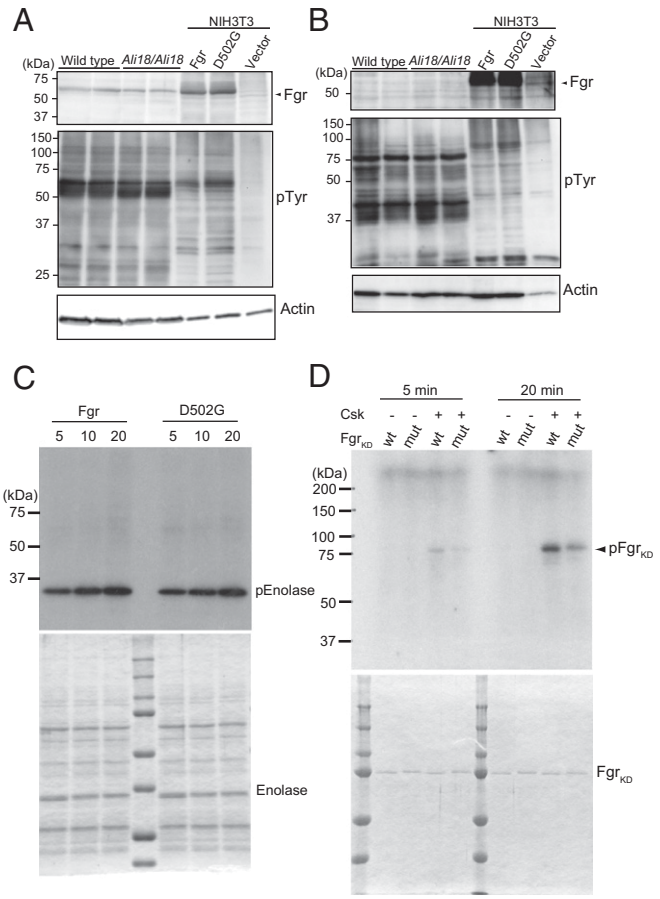

Fig. 3. Western blot analysis, tyrosine kinase assays, and phosphorylation of Fgr by C-terminal Src kinase (Csk). Cell lysate of spleen (*A*) and bone marrow cells (*B*) from wild-type and *Ali18/Ali18* mice were used for Western blotting. As control experiments, transformants of wild-type and p.Asp502Gly (D502G) Fgr expression constructs in murine embryo-derived cultured fibroblast, NIH 3T3, cells were used. Empty vector was transfected as negative control. Anti-Fgr (*Upper*), anti-phosphotyrosine (*Middle*), and anti-actin (*Lower*, loading control) were used. No overt changes in Fgr protein levels of *Ali18/Ali18* spleen (relative ratio: 0.900 ± 0.256, $P = 0.538$, *t* test) and NIH 3T3 cells (relative ratio: 0.982 ± 0.139, $P = 0.833$, *t* test) were detected. (*C*) In vitro translated wild-type and p.Asp502Gly Fgr proteins were used for kinase assay experiments. Recombinant enolase protein was used as SFK-specific substrate (*Lower*, loading control). No activity changes were detected in different reaction time. (*D*) The C-terminal phosphorylation of KD Fgr by Csk was measured. Fgr KD with p.Asp502Gly showed five and two times less phosphorylation levels in 5- and 20-min reaction time, respectively. The proteins used for kinase assays were fractionated by SDS/PAGE and stained by Coomassie Brilliant Blue. Experiments were independently triplicated.

experiments of PS show increased levels of phosphorylation compared with WT (relative activity ratio: 1.20 ± 0.05, $P = 0.015$, *t* test, Fig. 4 *I and J*). Unlike the *Ali18* mutation, the decreased levels of C-terminal phosphorylation of kinase dead RW and PS by Csk were not observed (Fig. 4*K*). However, both murine p.Arg106Trp (corresponding to PS) and p.Arg106Trp;p.Asp502Gly Fgr constructs showed an ∼10% decrease in C-terminal phosphorylation by Csk compared with the wild-type and p.Asp502Gly Fgr constructs, respectively (*SI Appendix*, Fig. S7).

Discussion

In this study, we identified *Fgr* as the causative gene for inflammatory disease in the *Ali18* mutant mice by positional candidate cloning despite complex modifier effects from the genetic background. Further genetic studies by genome editing confirmed that multiple null alleles of *Fgr* disrupt the inflammatory paw phenotype in *Ali18* mice. Previously, it was shown that the *Ali18* phenotype occurs independently of the adaptive immune system (disease occurs in *Ali18;Rag1*$^{-/-}$ mice that lack B and T cells); further, granulocytes are increased in peripheral blood of *Ali18* mice (18). Fgr is predominantly expressed in myeloid

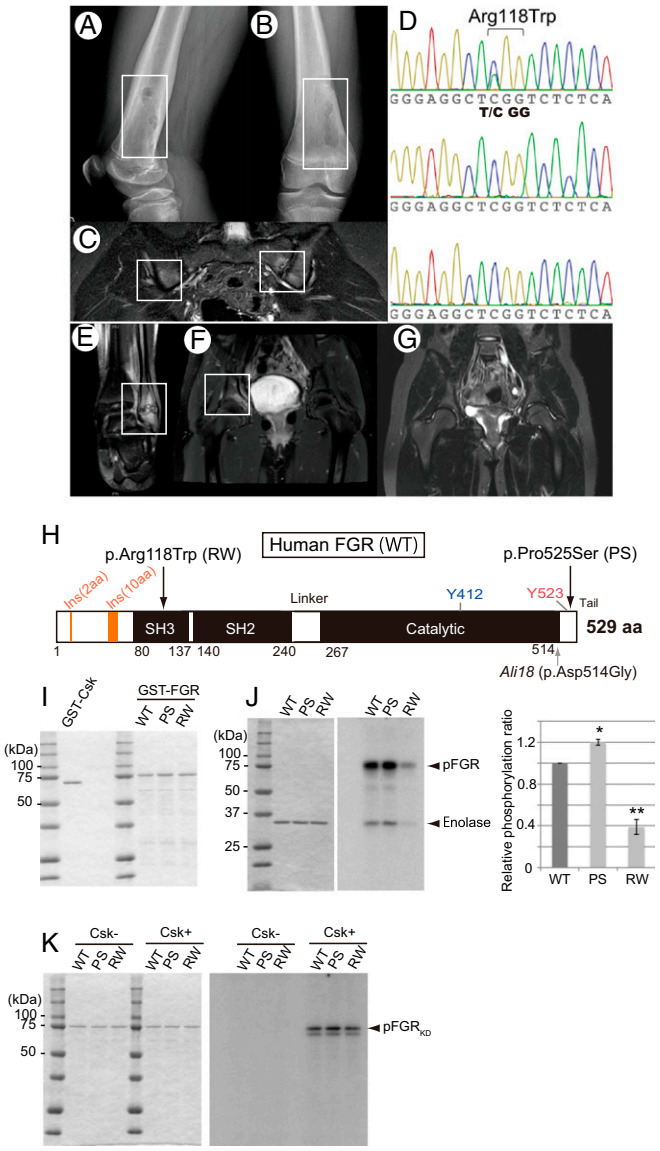

Fig. 4. Missense mutations of *FGR* in CRMO and phosphorylation assays. (*A* and *B*) Radiograph of case 1 (p.Arg118Trp). Osteolytic lesions with sclerosis and periosteal elevation of the right distal femur are shown. (*C*) MRI of case 1. Increased STIR signal intensity on the iliac and sacral sides of the left sacroiliac joints is shown. (*D*) Sanger sequencing chromatogram of p.Arg118Trp in the proband (*Top*), father (*Middle*), and mother (*Bottom*). Proband harbors a de novo C > T mutation, which induces a p.Arg118Trp amino acid change in *FGR*. (*E–G*) MRI of case 2 (p.Pro525Ser). Abnormalities included increased signal intensity on STIR images in the left distal fibula (*E*) and the pelvis at the right acetabulum (*F*). (*G*) Repeat MRI 9 mo after naproxen therapy showing improvement in the left acetabular lesion. (*H*) Schematic diagram of amino acid substitution from the *FGR* mutations found in human CRMO (*Top* arrows) and the mouse *Ali18* mutation (*Lower* arrow). (*I*) SDS/PAGE of affinity purified Csk and FGR used in kinase assays. (*J*) Kinase activity of FGR with CRMO variants. (*J*, *Left*) SDS/PAGE of affinity purified substrate, enolase, used in each assay. (*J*, *Right*) Phosphorylation intensity of enolase and FGR indicate enzyme activity. (*K*) Phosphorylation of FGR_{KD} with CRMO variants by Csk. (*Left*) SDS/PAGE of affinity purified FGR_{KD} of human CRMO variants as substrate used in each assay. (*Right*) FGR_{KD} proteins were phosphorylated by Csk in equal intensity. Experiments were independently triplicated.

lineage cells such as granulocytes, monocytes, and dendritic cells (29). This expression pattern fits the cell populations implicated in the autoinflammatory phenotype of *Ali18* mice. Because Fgr plays an important role in mast cell activation (30, 31) and neutrophil adhesion (29), these cell types are likely contributing independently, or in combination, to autoinflammation in *Ali18* mice and is the subject of ongoing research.

In SFKs, the C-terminal region is important for inactivation of tyrosine kinase activity; therefore defects in the C-terminal region cause constitutive activation, which leads to cancerization (32, 33). Csk is another member of SFKs and specifically phosphorylates a C-terminal tyrosine of SFKs (34). Without C-terminal phosphorylation by Csk, SFKs cannot form a folded inactive conformation. For this phosphorylation, it is known that docking between the C-terminal region of SFKs and Csk is necessary (27). In our results, $Fgr^{Asp502Gly}$ was less phosphorylated than wild-type Fgr by Csk. The corresponding amino acid substitution in Src (p.Asp518Ala) also shows decreased phosphorylation of the C-terminal region (27). Thus, it strongly suggests that constitutive activation of Fgr leads to the inflammatory phenotypes of *Ali18* mice.

In the *cmo* (*chronic multifocal osteomyelitis*) mouse model, the proinflammatory cytokine IL1-β mediates autoinflammation but does not require the Nlrp3 inflammasome (35). In Fgr^{Ali18} mice, IL1β is not up-regulated in peripheral blood (18). Although Fgr is not known to activate the inflammasome directly, NEK7 serine-threonine kinase and two tyrosine kinases, Btk and Syk, control inflammasome activation by phosphorylation (36). Thus, the phosphorylation network is important for regulation of inflammasome activation in myeloid cells. Recently, it was reported that phosphorylation of CBL ubiquitin ligase at Y371 by SFKs negatively controls NLRP3 inflammasome activation (37). Further, Cbl ubiquitinates Fgr directly for its activation (38). Thus, gain of function of Fgr may lead to the activation loop of Fgr-Cbl which suppresses the NLRP3 inflammasome. These suggest that autoinflammation caused by Fgr activation occurs independent of Nlrp3 inflammasome activation.

In the cohort of patients with CRMO, we found two *FGR* coding variants, p.Arg118Trp and p.Pro525Ser, which are located in the SH3 domain and C-terminal tail, respectively. Since decreased C-terminal phosphorylation by Csk was not observed using human *FGR* constructs, it is likely that mouse and human mutations have different functional properties. Increased kinase activation was observed in p.Pro525Ser FGR. Pro525 is the only hydrophobic amino acid in the C terminus of FGR. In the inactive form of Src, the C-terminal region is bound to two hydrophobic pockets of the protein surface in the SH2 domain (39, 40). The substitution of the substitution of Pro525 for hydrophilic Ser could be repellent to the surface of the hydrophobic binding pocket. Because the surface region is conserved between Src and Fgr (39), p.Pro525Ser FGR probably leads to instability of the inactive form. Thus, the active form of FGR could dominate the signaling cascade in the patient. In contrast, the role of p.Arg118Trp in CRMO pathogenesis remains difficult to define. The murine equivalent p.Arg106Trp mutation showed a decrease in phosphorylation versus wild-type murine Fgr, yet in vitro functional studies of p.Arg118Trp in human, constructs showed decreased kinase activity. Since human FGR has additional amino acid residues at the N terminus (amino acid residues 14–15 and 49–58; Fig. 4*H*) compared with murine Fgr, we hypothesize that these structural differences in FGR influence C-terminal phosphorylation. As described in *Results*, *Ali18_#*408a (p.Ser25Arg;Asp502Gly) mice exhibited more severe inflammatory phenotypes; this genetic model supports the importance of C- and N-terminal interactions in Fgr function. While the de novo status of the p.Arg118Trp mutation strongly supports its pathogenicity, in the absence of additional human CRMO cases with the same mutation, *Fgr* p.Arg106Trp mutant mice or *FGR* p.Arg118Trp knockin mice are needed to better determine the role of this mutation in sterile bone inflammation.

The genetic etiology of most sporadic CRMO cases is not yet known and it is likely that variants at multiple loci, in addition to environmental factors, both contribute together to disease development. We queried sequence data from the 13 CRMO probands with *FGR* coding variants for additional protein coding changes in the other CRMO candidate genes. A p.Gly311Arg change in *FBLIM1* was identified in two probands and a p.Cys874Phe change in *LPIN2* was identified in one proband. The *FBLIM1* variant is not rare, with a minor allele frequency of 0.0195 in gnomAD and is in the FERMT2-binding domain, not the filamin-binding domain as was the variant previously reported (41). Phosphorylation of FERMT2 by Src facilitates interaction of FERMT2 with FBLIM1, and this complex then is recruited to focal adhesions as part of integrin-mediated cellular signaling (42). The concurrent and compound heterozygous status of both *FGR* and *FBLIM1* variants in CRMO probands is supportive of genetic interactions between the two genes and future experiments will verify if variants in FGR or FBLIM1 found in CRMO patients disrupt this feedback loop. Regarding the *LPIN2* missense variant, to date there is no established interaction between LIPIN2 and FGR.

We experimentally showed that inactivation of *Fgr* by genome editing abolished autoinflammatory bone and joint disease in *Fgr* p.Asp502Gly mutant *Ali18* mice. This suggests targeting FGR function would be of potential therapeutic benefit in humans with autoinflammatory phenotypes. Tyrosine kinase inhibitors effective against SFK, including PP1, PP2, and dasatinib (43, 44), are therapeutic candidates. In particular, dasatinib relieves bone pain in animal models of cancer-induced bone pain (45). Such small molecule inhibitors may be effective on other members of SFKs, by targeting the ATP binding domain; however, this increases the likelihood of side effects. Recently, however, the FGR-specific inhibitor, TL02-59, has been identified as a suppressor of acute myelogenous leukemia cell growth (46). Testing these therapies in *Ali18* mice will help determine the effectiveness of SFK inhibitors as a potential therapeutic target for the treatment of CRMO and other inflammatory diseases.

In conclusion, we identified the tyrosine kinase FGR as a functional intracellular signaling molecule involved in the pathogenesis of autoinflammatory bone diseases. Dysregulation of active–inactive conformational changes in FGR protein leads to osteomyelitis in mice and humans. Thus, trial and development of SFK inhibitors using the animal model will provide insights into the potential for therapeutic options in the treatment of human CRMO.

Methods

Mice. The *Ali18* strain (C3HeB/FeJ-Mhdaali18) was established in the Munich mouse ENU mutagenesis project (47), and its character and maintenance have been described previously (17, 19). For genotyping of the *Fgr* locus of *Ali18* mice, see *SI Appendix, Methods*. All animal care and experimental protocols using mice were conducted in accordance with the Tokai University Institutional Animal Care and Use Committee, and all animal research was approved by this committee before the experiments.

Positional Candidate Cloning. Standard genetic mapping was used to narrow down the critical region (17, 19). In the region, we used a literature-based search engine, PosMed (20), to select candidate genes. Because bone marrow cells from *Ali18* mice could reconstitute the inflammatory phenotype of *Ali18* mice in irradiated wild-type mice (18), we used "bone marrow" as a keyword for search by PosMed. Sixteen genes were selected, and PCR primer pairs spanning the exonic region were designed by ExonPrimer (https://ihg.helmholtz-muenchen.de). The PCR products from wild-type and *Ali18*/*Ali18* templates were then sequenced by standard Sanger sequencing.

Genome Editing of *Ali18* Mice. A standard DNA microinjection method into *Ali18*/*Ali18* fertilized eggs was performed (48) using pX330-based constructs described in *SI Appendix, Methods*. To obtain *Ali18*/*Ali18* fertilized eggs, in vitro fertilization with *Ali18*/*Ali18* oocyte and sperm was done. The CRISPR/Cas9-mediated mutations of F0 and F1 mice were confirmed by Sanger sequencing. We only used F0 mice (*Ali18*/*Ali18*) with newly introduced mutations in exon 3 of *Fgr* for further mating with C3HeB/FeJ mice to obtain F1 mice (*Ali18*/+).

Western Blotting. Western blotting was done by a standard procedure as previously described (49). Antibodies used in this study were as follows: anti-Fgr (M60) (sc-50338, Santa Cruz Biotechnology, Inc.), anti-phosphotyrosine (06–427, Upstate), and anti-actin (A5471, Sigma). For protein preparation from tissues and cultured cells, see *SI Appendix, Methods*.

Protein Purification for Kinase Assays. The in vitro transcription/translation system was used to synthesize mouse Fgr protein (TNT Quick Systems, Promega). GST-Csk (mouse), GST-Fgr_{KD} (mouse), and GST-FGR and GST-FGR_{KD} (human) were expressed in *Escherichia coli* BL21(DE3), purified by glutathione

Sepharose 4B (GE Healthcare), and stored in 50 mM Tris·HCl, pH 8.0, at −80 °C. Purity of the purified proteins was examined by SDS-polyacrylamide gel electrophoresis and Coomassie Brilliant Blue (CBB) staining. Protein concentrations were determined by using a Pierce BCA Protein Assay Kit (Thermo Scientific). For the phosphorylation assay procedures, see *SI Appendix, Methods*.

Clinical Samples and Exome Sequencing. All human research was approved by the University of Iowa Institutional Review Board. Written informed consent was obtained from all clinical study participants and written parental or guardian consent was obtained, because all participants were under the age of 18. Use of clinical samples, whole-exome sequencing, and data analysis is described previously in detail (41), although more recent Agilent exome platforms (V5 and V6+UTR) were used for 8/99 samples (V5) and 79/99 (V6+UTR) samples.

ACKNOWLEDGMENTS. We thank Kumiko Ishikawa, Maya Tanigawa, Miyu Hirano, Miyuki Kitabayashi, Kumiko Sugizaki, and Hideo Tsukamoto for excellent technical assistance. We are also thankful to Sanae Ogiwara, Ayaka Nakamura, and Yutaka Ishikawa for mouse embryo manipulation. This work was supported in part by grants from Japan Society for the Promotion of Science (JSPS 19500370 and 22500392), Takeda Science Foundation, and Research Foundation of Ituu to K.A., German Federal Ministry of Education and Research (Infrafrontier Grant 01KX1012 to M.H.d.A.), the National Institutes of Health (National Institute of Arthritis, Musculoskeletal and Skin R01AR059703 to P.J.F. and A.G.B.). V.B.M. and A.G.B. are supported by NIH Grants (R01EY026682, R01EY024665, R01EY025225, R01EY024698, and R21A050437), the Doris Duke Charitable Foundation Grant 2013103, and Research to Prevent Blindness New York, NY. G.V. is supported by NIH Grants (F30EYE027986 and T32GM997337).

1. S. L. Masters, A. Simon, I. Aksentijevich, D. L. Kastner, Horror autoinflammaticus: The molecular pathophysiology of autoinflammatory disease (*). *Annu. Rev. Immunol.* **27**, 621–668 (2009).
2. A. Jansson *et al.*, Classification of non-bacterial osteitis: Retrospective study of clinical, immunological and genetic aspects in 89 patients. *Rheumatology (Oxford)* **46**, 154–160 (2007).
3. P. J. Ferguson, M. Sandu, Current understanding of the pathogenesis and management of chronic recurrent multifocal osteomyelitis. *Curr. Rheumatol. Rep.* **14**, 130–141 (2012).
4. S. R. Hofmann *et al.*, Chronic recurrent multifocal osteomyelitis (CRMO): Presentation, pathogenesis, and treatment. *Curr. Osteoporos. Rep.* **15**, 542–554 (2017).
5. M. R. Roderick, E. S. Sen, A. V. Ramanan, Chronic recurrent multifocal osteomyelitis in children and adults: Current understanding and areas for development. *Rheumatology (Oxford)* **57**, 41–48 (2018).
6. P. J. Ferguson *et al.*, Homozygous mutations in LPIN2 are responsible for the syndrome of chronic recurrent multifocal osteomyelitis and congenital dyserythropoietic anaemia (Majeed syndrome). *J. Med. Genet.* **42**, 551–557 (2005).
7. I. Aksentijevich *et al.*, An autoinflammatory disease with deficiency of the interleukin-1-receptor antagonist. *N. Engl. J. Med.* **360**, 2426–2437 (2009).
8. K. Abe, P. Yu, Positional cloning in mice and its use for molecular dissection of inflammatory arthritis. *Curr. Pharm. Biotechnol.* **10**, 252–260 (2009).
9. J. Grosse *et al.*, Mutation of mouse Mayp/Pstpip2 causes a macrophage autoinflammatory disease. *Blood* **107**, 3350–3358 (2006).
10. L. Byrd, M. Grossmann, M. Potter, G. L. Shen-Ong, Chronic multifocal osteomyelitis, a new recessive mutation on chromosome 18 of the mouse. *Genomics* **11**, 794–798 (1991).
11. P. J. Ferguson *et al.*, A missense mutation in pstpip2 is associated with the murine autoinflammatory disorder chronic multifocal osteomyelitis. *Bone* **38**, 41–47 (2006).
12. N. Sakaguchi *et al.*, Altered thymic T-cell selection due to a mutation of the ZAP-70 gene causes autoimmune arthritis in mice. *Nature* **426**, 454–460 (2003).
13. P. Yu *et al.*, Autoimmunity and inflammation due to a gain-of-function mutation in phospholipase C gamma 2 that specifically increases external Ca2+ entry. *Immunity* **22**, 451–465 (2005).
14. K. Abe *et al.*, A novel N-ethyl-N-nitrosourea-induced mutation in phospholipase Cγ2 causes inflammatory arthritis, metabolic defects, and male infertility in vitro in a murine model. *Arthritis Rheum.* **63**, 1301–1311 (2011).
15. M. J. Ombrello *et al.*, Cold urticaria, immunodeficiency, and autoimmunity related to PLCG2 deletions. *N. Engl. J. Med.* **366**, 330–338 (2012).
16. Q. Zhou *et al.*, A hypermorphic missense mutation in PLCG2, encoding phospholipase Cγ2, causes a dominantly inherited autoinflammatory disease with immunodeficiency. *Am. J. Hum. Genet.* **91**, 713–720 (2012).
17. K. Abe, H. Fuchs, T. Lisse, W. Hans, M. Hrabe de Angelis, New ENU-induced semidominant mutation, Ali18, causes inflammatory arthritis, dermatitis, and osteoporosis in the mouse. *Mamm. Genome* **17**, 915–926 (2006).
18. K. Abe *et al.*, Novel lymphocyte-independent mechanisms to initiate inflammatory arthritis via bone marrow-derived cells of Ali18 mutant mice. *Rheumatology (Oxford)* **47**, 292–300 (2008).
19. K. Abe *et al.*, Genome-wide search for genes that modulate inflammatory arthritis caused by Ali18 mutation in mice. *Mamm. Genome* **20**, 152–161 (2009).
20. Y. Yoshida *et al.*, PosMed (Positional Medline): Prioritizing genes with an artificial neural network comprising medical documents to accelerate positional cloning. *Nucleic Acids Res.* **37**, W147–W152 (2009).
21. G. Naharro *et al.*, Molecular cloning of integrated Gardner-Rasheed feline sarcoma virus: Genetic structure of its cell-derived sequence differs from that of other tyrosine kinase-coding onc genes. *J. Virol.* **47**, 611–619 (1983).
22. M. T. Brown, J. A. Cooper, Regulation, substrates and functions of src. *Biochim. Biophys. Acta* **1287**, 121–149 (1996).
23. S. Timmermans, M. Van Montagu, C. Libert, Complete overview of protein-inactivating sequence variations in 36 sequenced mouse inbred strains. *Proc. Natl. Acad. Sci. U.S.A.* **114**, 9158–9163 (2017).
24. Y. Choi, G. E. Sims, S. Murphy, J. R. Miller, A. P. Chan, Predicting the functional effect of amino acid substitutions and indels. *PLoS One* **7**, e46688 (2012).
25. C. A. Lowell, P. Soriano, H. E. Varmus, Functional overlap in the src gene family: Inactivation of hck and fgr impairs natural immunity. *Genes Dev.* **8**, 387–398 (1994).
26. C. A. Lowell, P. Soriano, Knockouts of Src-family kinases: Stiff bones, wimpy T cells, and bad memories. *Genes Dev.* **10**, 1845–1857 (1996).
27. S. Lee, M. K. Ayrapetov, D. J. Kemble, K. Parang, G. Sun, Docking-based substrate recognition by the catalytic domain of a protein tyrosine kinase, C-terminal Src kinase (Csk). *J. Biol. Chem.* **281**, 8183–8189 (2006).
28. M. Lek *et al.*; Exome Aggregation Consortium Analysis of protein-coding genetic variation in 60,706 humans. *Nature* **536**, 285–291 (2016).
29. C. A. Lowell, Src-family kinases: Rheostats of immune cell signaling. *Mol. Immunol.* **41**, 631–643 (2004).
30. J. H. Lee *et al.*, The Src family kinase Fgr is critical for activation of mast cells and IgE-mediated anaphylaxis in mice. *J. Immunol.* **187**, 1807–1815 (2011).
31. R. Suzuki *et al.*, Molecular editing of cellular responses by the high-affinity receptor for IgE. *Science* **343**, 1021–1025 (2014).
32. S. A. Courtneidge, Activation of the pp60c-src kinase by middle T antigen binding or by dephosphorylation. *EMBO J.* **4**, 1471–1477 (1985).
33. J. A. Cooper, K. L. Gould, C. A. Cartwright, T. Hunter, Tyr527 is phosphorylated in pp60c-src: Implications for regulation. *Science* **231**, 1431–1434 (1986).
34. M. Okada, Regulation of the SRC family kinases by Csk. *Int. J. Biol. Sci.* **8**, 1385–1397 (2012).
35. S. L. Cassel *et al.*, Inflammasome-independent IL-1β mediates autoinflammatory disease in Pstpip2-deficient mice. *Proc. Natl. Acad. Sci. U.S.A.* **111**, 1072–1077 (2014).
36. T. Gong, W. Jiang, R. Zhou, Control of inflammasome activation by phosphorylation. *Trends Biochem. Sci.* **43**, 685–699 (2018).
37. I. C. Chung *et al.*, Src-family kinase-Cbl axis negatively regulates NLRP3 inflammasome activation. *Cell Death Dis.* **9**, 1109 (2018).
38. F. Melander, T. Andersson, K. Dib, Fgr but not Syk tyrosine kinase is a target for beta 2 integrin-induced c-Cbl-mediated ubiquitination in adherent human neutrophils. *Biochem. J.* **370**, 687–694 (2003).
39. G. Waksman *et al.*, Crystal structure of the phosphotyrosine recognition domain SH2 of v-src complexed with tyrosine-phosphorylated peptides. *Nature* **358**, 646–653 (1992).
40. G. Waksman, S. E. Shoelson, N. Pant, D. Cowburn, J. Kuriyan, Binding of a high affinity phosphotyrosyl peptide to the Src SH2 domain: Crystal structures of the complexed and peptide-free forms. *Cell* **72**, 779–790 (1993).
41. A. J. Cox *et al.*, Recessive coding and regulatory mutations in FBLIM1 underlie the pathogenesis of chronic recurrent multifocal osteomyelitis (CRMO). *PLoS One* **12**, e0169687 (2017).
42. Z. Liu *et al.*, Kindlin-2 phosphorylation by Src at Y193 enhances Src activity and is involved in Migfilin recruitment to the focal adhesions. *FEBS Lett.* **589**, 2001–2010 (2015).
43. J. H. Hanke *et al.*, Discovery of a novel, potent, and Src family-selective tyrosine kinase inhibitor. Study of Lck- and FynT-dependent T cell activation. *J. Biol. Chem.* **271**, 695–701 (1996).
44. T. O'Hare *et al.*, Inhibition of wild-type and mutant Bcr-Abl by AP23464, a potent ATP-based oncogenic protein kinase inhibitor: Implications for CML. *Blood* **104**, 2532–2539 (2004).
45. C. K. Appel *et al.*, The Src family kinase inhibitor dasatinib delays pain-related behaviour and conserves bone in a rat model of cancer-induced bone pain. *Sci. Rep.* **7**, 4792 (2017).
46. M. C. Weir *et al.*, Selective inhibition of the myeloid Src-family kinase Fgr potently suppresses AML cell growth in vitro and in vivo. *ACS Chem. Biol.* **13**, 1551–1559 (2018).
47. M. Hrabe de Angelis *et al.*, Genome-wide, large-scale production of mutant mice by ENU mutagenesis. *Nat. Genet.* **25**, 444–447 (2000).
48. M. Hogan, R. Beddingtom, F. Constantini, E. Lacy, *Manipulating the Mouse Embryo* (Cold Spring Harbor Laboratory Press, New York, ed. 2, 1994).
49. K. Abe *et al.*, Novel ENU-induced mutation in Tbx6 causes dominant spondylocostal dysostosis-like vertebral malformations in the rat. *PLoS One* **10**, e0130231 (2015).